Journal of Solid State Chemistry **157,** 94–101 (2001)
doi:10.1006/jssc.2000.9043, available online at http://www.idealibrary.com on IDEAL®

Formation by Laser Impact of Conducting β-Ga_2O_3–In_2O_3 Solid Solutions with Composition Gradients

C. Vigreux, L. Binet,[1] and D. Gourier

Laboratoire de Chimie Appliquée de l'Etat Solide, UMR CNRS 7574, Ecole Nationale Supérieure de Chimie de Paris, 11, rue Pierre et Marie Curie, F-75231 Paris cedex 05, France

and

B. Piriou

Laboratoire des Structures, Propriétés et Modélisation du Solide, UMR CNRS 8580, Ecole Centrale de Paris, Grande Voie des Vignes, F-92295 Chatenay-Malabry cedex, France

Solid solutions of β-$Ga_{2-2x}In_{2x}O_3$ ($x \leq 0.4$) with β-gallia structure were investigated by Raman spectroscopy. A continuous evolution with a linear shift of the Raman lines with increasing x was observed in the existence range of the solid solution ($x \leq 0.4$). For $0.4 \leq x \leq 0.5$, strong alterations of the Raman spectra were observed, corresponding either to the demixing of the solid solutions for the samples elaborated at 1400°C or to the occurrence of a new phase with κ-alumina structure for samples elaborated at 1550°C. The *in situ* formation of the β-$Ga_{2-2x}In_{2x}O_3$ compounds under laser irradiation could also be followed by Raman spectroscopy. Strong local variations of composition caused by a heterogeneous loss of indium could be detected inside the irradiated areas. In addition electron paramagnetic resonance revealed the existence of conduction electrons in these areas, resulting from a slight oxygen deficiency. These gradients of composition induce a spatial variation of the band gap and of the position of the Fermi level with respect to the conduction band so that the system is equivalent to an intrinsic/n-type junction.

Key Words: **gallium–indium oxide; laser-induced crystallization; composition gradients; Raman spectroscopy.**

INTRODUCTION

Solid solutions of $Ga_{2-2x}In_{2x}O_3$ ($x \leq 0.4$) with β-Ga_2O_3 structure have recently attracted an increasing interest as potential transparent conducting oxides (TCO) in optoelectronic devices (1), because these compounds combine a wide band gap and n-type semiconduction due to oxygen vacancies (1, 2). The β-Ga_2O_3 structure contains both tetrahedral and octahedral cation sites. However In^{3+} ions in β-$Ga_{2-2x}In_{2x}O_3$ solid solutions are preferentially located in octahedral sites (3, 4). The participation of both indium 5*s* and 5*p* atomic orbitals to the conduction band edge enables a tunability of the optical properties of these compounds by varying the indium concentration (5). Although much information is now available about the phase diagram of the binary system Ga_2O_3–In_2O_3 (3, 6) and about the optical and the electronic properties of the β-$Ga_{2-2x}In_{2x}O_3$ solid solutions (1, 2, 5), nothing is known about the formation of these compounds. It may be important to investigate this point since disorder appearing during the elaboration of the samples may induce a nonreproductibility of the electronic properties (5). Valuable information about the structure and the disorder in solids can be obtained from vibrational Raman spectroscopy. However, to our knowledge, only β-Ga_2O_3 has been studied by this technique (7). Therefore, the first aim of this paper is to present a Raman investigation of the β-$Ga_{2-2x}In_{2x}O_3$ compounds. The second aim consists of studying the formation of these compounds or the changes induced in preformed compounds by heating locally an initial powder with a laser beam. The strong temperature gradients due to the local laser heating should induce spatial variations of composition and of electronic properties that can be probed by Raman and electron paramagnetic resonance (EPR) spectroscopies.

EXPERIMENTAL

The β-$Ga_{2-2x}In_{2x}O_3$ compounds analyzed by Raman spectroscopy were prepared by coprecipitation before annealing. This method provides more intimate mixing of the raw materials than solid state reaction. Gallium metal was dissolved in HNO_3 at 60°C and stirred overnight to obtain

[1] To whom correspondence should be addressed.

0022-4596/01 $35.00

a clear solution, and $[In(NO_3)_2,5H_2O]$ was dissolved in water. Both metal solutions were poured with stirring in an aqueous ammonia solution. After heating the resulting powders became white or yellow, depending on the mole fraction of indium. After calcination at 400°C to evaporate NH_4NO_3, the powders were ground and pressed into pellets. One series of pellets was then heated at 1400°C for 2 h and another one was heated at 1550°C for 15 h.

The study of the formation of the β-$Ga_{2-2x}In_{2x}O_3$ solid solutions under laser annealing was performed on initial powders either amorphous or crystallized. In the first case the amorphous powder was obtained by coprecipitation. In the second case the crystallized powder was prepared by sintering a mixture of crystalline Ga_2O_3 and In_2O_3 powders at 1000°C for 5 h. This temperature was low enough to avoid the formation of the β-$Ga_{2-2x}In_{2x}O_3$ solid solution. Then the formation of the β-$Ga_{2-2x}In_{2x}O_3$ compounds was induced by a laser irradiation with a multiline argon ion laser. This method allows a local heating so that heated and nonheated areas can be compared. We also studied the laser-induced recrystallization of preformed β-$Ga_{2-2x}In_{2x}O_3$ compounds. The latter were obtained by heating at 1200°C for 2 h of an initial powder either prepared by coprecipitation or by mixture of Ga_2O_3 and In_2O_3 powders.

Room temperature Raman scattering spectra were obtained with a Spectra Physics argon ion laser (Model 2000) as excitation source. The 514.5-nm line was mainly used. In a 90° geometry the scattered radiation was dispersed by a Jobin-Yvon ISA T800 triple monochromator and detected with a Hamamatsu R464 photomultiplier. The experimental setup included a photon counting and a computer for data acquisition and treatment. Depending on the recorded spectral range the scan rate was chosen between 1 and 50 cm^{-1} and the band width in the range 3 to 1 cm^{-1}.

Room temperature micro-Raman scattering spectra were recorded on a LABRAM 1 instrument from Dilor Company (ISA) equipped with a He–Ne laser (632.8 nm) and a Spectra Physics argon ion laser (Model 2000). The 514.5-nm line of the latter was mainly used. A microscope lens $\times 50$ focused the laser beam onto the sample located in the focal plane of the microscope. A two-dimensional CCD detector at the exit port of the spectrometer collected both spatial and spectral information originating from the illuminated area of the sample.

EPR spectra were recorded with an X-band (9.4 GHz) ESP300e Bruker spectrometer equipped with a TE_{102} cavity and a variable temperature device.

RAMAN ANALYSIS OF THE SOLID SOLUTIONS

Before analyzing the Raman spectra of the β-$Ga_{2-2x}In_{2x}O_3$ compounds, it is useful to recall the main features of the phase diagram of the system Ga_2O_3–In_2O_3. X-ray diffraction showed the existence of the β-gallia phase $Ga_{2-2x}In_{2x}O_3$ up to $x = 0.4$ (3). For $0.4 < x \leq 0.5$, the system demixes into a β-gallia phase with $x = 0.4$ and a cubic solid solution Ga_2O_3–In_2O_3 with In_2O_3 structure for low temperature (1200°C) heat treatment (3). A thermal treatment at higher temperature (1550°C) yields a single phase with κ-alumina structure replacing the β-gallia phase (8, 9).

The β-gallia structure belongs to the $C2/m$ space group. A complete vibrational study of β-Ga_2O_3 was previously performed by Dohy *et al.* (7). The phonon modes at the center of the Brillouin zone are distributed as follows:

$$\Gamma_m = 10\ A_g + 5\ B_g + 10\ B_u + 5\ A_u \qquad [1]$$

in which the 10 A_g modes and the 5 B_g modes are Raman active. Figure 1a shows the 15 Raman transitions of a

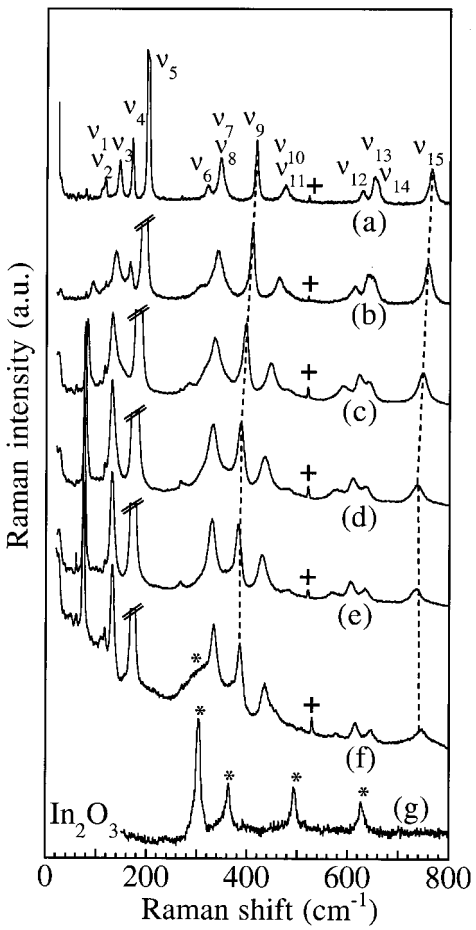

FIG. 1. Raman spectra of coprecipitated $Ga_{2-2x}In_{2x}O_3$ solid solutions heated 2 h at 1400°C with (a) $x = 0$; (b) $x = 0.1$; (c) $x = 0.2$; (d) $x = 0.3$; (e) $x = 0.4$; and (f) $x = 0.5$ and showing a β-gallia structure. The star on spectrum (f) indicates a line characteristic of a cubic solid solution of Ga_2O_3 into In_2O. (g) Raman spectrum of polycrystalline In_2O_3 obtained with the 632.8 Å line of the He–Ne. The narrow line at 520.4 cm^{-1} (+) is a plasma laser line.

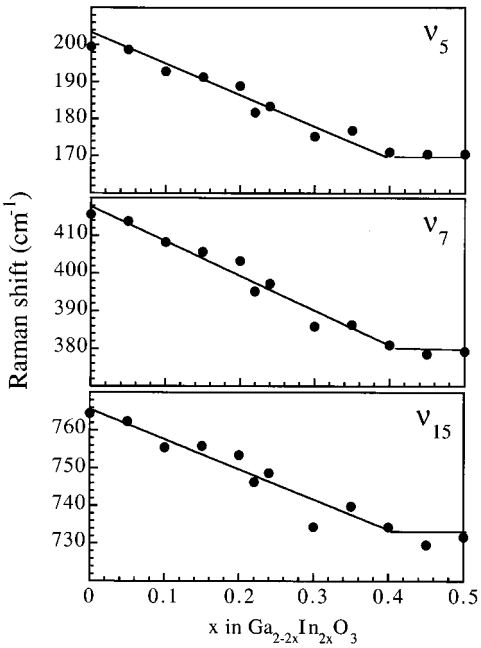

FIG. 2. Raman shifts versus x for the 199, 415, and 760 cm^{-1} modes.

β-Ga_2O_3 polycrystalline sample obtained by coprecipitation. Some of these transitions overlap and are not resolved (ν_7 and ν_8 on the one hand and ν_{13} and ν_{14} on the other hand). The Raman line at 199 cm^{-1} (ν_5) is particularly strong. Renormalization of the spectrum by the term $\nu/(n+1)$ (10) with n being the Bose–Einstein factor gives the spectrum at 0 K in which the line at 763 cm^{-1} (ν_{15}) also turns out to be strong.

Raman spectra of the various Ga_2O_3–In_2O_3 solid solutions treated 2 h at 1400°C present the characteristic lines of the β-gallia phase up to $x = 0.5$, as shown in Fig. 1. For $x = 0.5$ (Fig. 1f), an extra line indicated by a star appears as a shoulder at about 300 cm^{-1} in the ν_7/ν_8 line. This broad line could be related to the strongest line of the Raman spectrum of In_2O_3 (Fig. 1g). This feature agrees with the

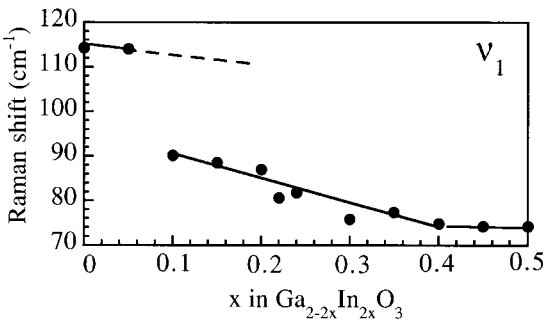

FIG. 3. Raman shift of the ν_1 line versus x showing a two-mode behavior.

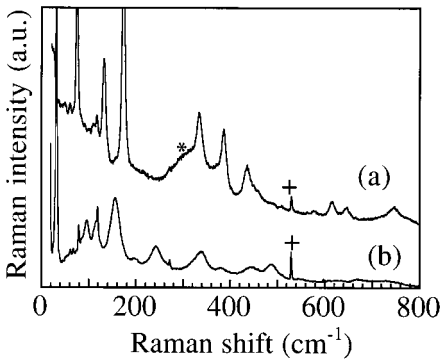

FIG. 4. Raman spectra of coprecipitated solid solutions with $x = 0.5$: (a) after a 2-h heat treatment at 1400°C, revealing a β-gallia structure with $x = 0.4$ and a cubic solid solution of Ga_2O_3 into In_2O_3 indicated by a star; (b) after a 15-h heat treatment at 1550°C, revealing a single phase with κ-alumina structure.

existence of a Ga_2O_3–In_2O_3 solid solution with the In_2O_3 structure resulting from the demixing of β-$Ga_{2-2x}In_{2x}O_3$ for $x > 0.4$ as revealed by X-ray diffraction (3). Substitution of gallium by indium shifts all the lines of β-Ga_2O_3 to low frequencies (Figs. 1a–1f). Most lines follow a "one-mode" behavior as their frequencies decrease linearly with the indium content up to $x = 0.4$, as illustrated in Fig. 2. The low-frequency shift of the Raman lines observed upon increasing x is related to the higher mass of In compared to that of Ga (respectively, 114.8 g mol^{-1} and 69.7 g mol^{-1}). For $x > 0.4$, the lines do not shift anymore, which is in good agreement with the coexistence of the two phases revealed by X-ray diffraction (3). However, one Raman line (ν_1 on Fig. 1a) follows a "two-mode" behavior, as shown in Fig. 3. This behavior is often observed when the masses of the two cations are very different, which is the case with Ga and In (11). It is quite surprising that this behavior is not observed with any other lines.

The relative shift $(\nu(x=0) - \nu(x=0.4))/\nu(x=0)$ is more pronounced for the low-frequency lines ($\nu(x=0) <$ 320 cm^{-1}) than for the high-frequency lines ($\nu(x=0) >$ 320 cm^{-1}), with relative shifts in the range 0.09 to 0.13% in the first case and in the range 0.03 to 0.08% in the second case. The higher relative shift of the low-frequency lines can be easily understood since cation motions are more involved in low-frequency modes than in high-frequency ones as was shown in the valence force field calculations (7), so that substitution of Ga by In has more effect at low frequency.

The Raman spectra recorded on samples treated 15 h at 1550°C are still characteristic of a β-gallia phase up to $x = 0.4$. However, the lines are slightly narrower than those of the samples treated at 1400°C. This feature is explained by a better crystallinity of the samples treated at 1500°C, as confirmed by X-ray diffraction. In addition, the relative shifts of the Raman spectra modes are less significant in this

case, which indicates a loss of indium during the annealing treatment at 1550°C.

The Raman spectra recorded on samples with $x = 0.45$ and $x = 0.5$ heated 15 h at 1550°C exhibit a new set of lines (Fig. 4). These lines can be attributed to the phase with κ-alumina structure since the latter is observed by X-ray diffraction under these processing conditions (8, 9).

The results obtained by Raman spectroscopy are thus consistent with the phase diagram of the system Ga_2O_3–In_2O_3 deduced from X-ray diffraction (3, 6, 8, 9).

FORMATION OF THE β-$Ga_{2-2x}In_{2x}O_3$ SOLID SOLUTIONS BY LASER IMPACT

The *in situ* formation of the β-gallia phase under the focused irradiation of the argon ion laser (514.5-nm line) was followed by Raman spectroscopy. Amorphous coprecipitated powders were placed on the Raman sample holder and different Raman spectra were recorded after increasing laser irradiation times. For samples with low indium contents ($x = 0$ and $x = 0.1$), the β-gallia phase could be formed provided the irradiations were performed with a power higher than about 3 W. However, crystallization occurred so rapidly that it was impossible to follow the different stages of the phase formation. On the other hand, it was possible to follow the formation of the β-gallia phases for higher indium content ($x \geq 0.2$). Figure 5 shows characteristic Raman spectra recorded at different stages of the formation of the solid solution with an initial indium content of 30%. No Raman line could be observed before laser irradiation (Fig. 5a). The strongest lines characteristic of the solid solution appeared after a first irradiation at 600 mW for 2 min (Fig. 5b). The lines grow (Fig. 5c) and shift to higher wavenumbers (Fig. 5d) for irradiations at stronger power. This indicates an ordering of the β-gallia structure and a loss of indium during the laser heating. For the sake of comparison, Fig. 5e shows the Raman spectrum of an $x = 0.3$ β-gallia phase obtained by thermal treatment (2 h at 1400°C) of a coprecipitated amorphous powder. The linewidths were larger after laser irradiation than after a thermal treatment; this indicates that the former treatment leads to disordered β-gallia phases with a significant loss of indium, as shown by the shift of the Raman lines to high wavenumbers.

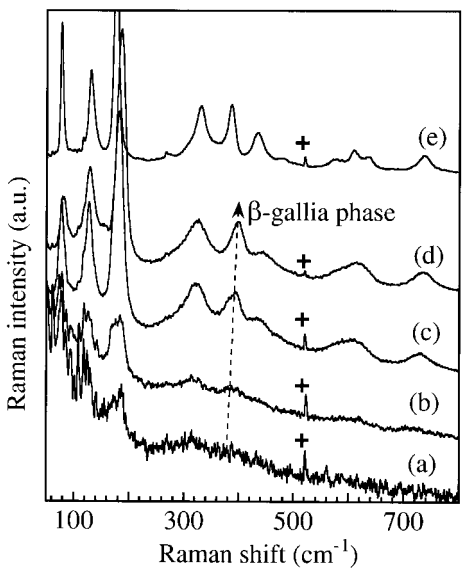

FIG. 5. Raman spectra of an initial amorphous powder $Ga_{2-2x}In_{2x}O_3$ with $x = 0.30$ recorded at 400 mW: before irradiation (a) and after an *in situ* irradiation by the laser of the Raman spectrometer at powers $P = 600$ mW (b), $P = 1$ W (c), and $P = 1.5$ W (d). Spectrum (e) corresponding to a coprecipitated sample with $x = 0.30$ and heated 2 h at 1400°C is shown for comparison.

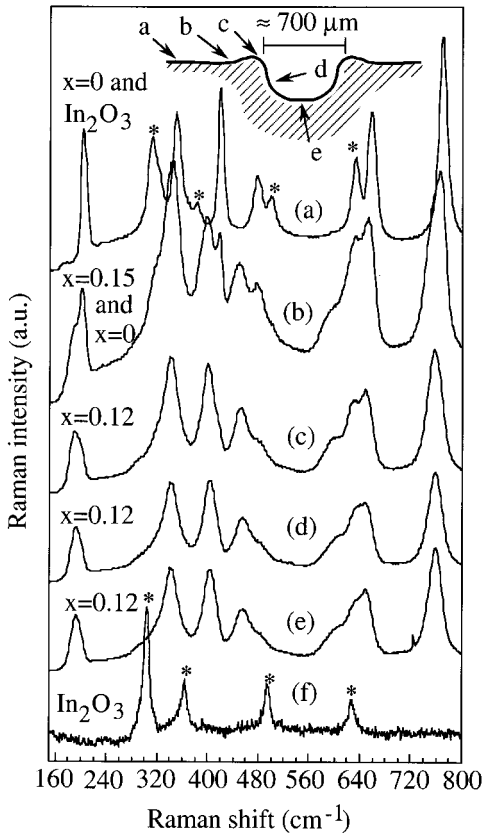

FIG. 6. Study of the melted hole created by laser irradiation of a mixture of crystallized powders of Ga_2O_3 (80%) and In_2O_3 (20%) heated 5 h at 1000°C. The profile of the hole (approximate diameter, 700 μm) is presented at the top of the figure and the letters a to e indicate the areas where the Raman spectra (a) to (e) were respectively recorded. The stars on spectrum (a) correspond to a cubic phase of In_2O_3. (f) Raman spectrum of polycrystalline In_2O_3.

The laser irradiation is also able to give β-$Ga_{2-2x}In_{2x}O_3$ phases from mixtures of polycrystalline Ga_2O_3 and In_2O_3 powders. These powders were first pressed into pellets and heated 5 h at 1000°C. This thermal treatment was chosen in

order to sinter the pellets without introducing indium into the β-Ga_2O_3 phase. The pellets were then locally irradiated by a focused 6-W multiline argon ion laser emission, which gave a blue hollow spot, and the as-obtained melted holes were studied by Raman microspectroscopy. Figure 6 summarizes the results obtained on a mixture of Ga_2O_3 (80%) and In_2O_3 (20%) crystalline powders. First it can be noticed that the lines' intensities are very different from those obtained by Raman spectroscopy. Such a difference is due to the different spectral sensitivities of the respective Raman and micro-Raman detectors. The inset at the top of Fig. 6 represents the profile of the hole created under irradiation, and letters a to e indicate the different areas where a micro-Raman spectrum was recorded. Outside the melted hole (Fig. 6a), the spectrum is characteristic of a biphasic system made up of the β-Ga_2O_3 phase and the In_2O_3 cubic phase (the spectrum of In_2O_3 is shown for comparison at the bottom of Fig. 6). This spectrum actually proved that a heat treatment at 1000°C of the powders obtained by solid state reaction did not allow the introduction of indium into the β-gallia phase. Close to the hole, the spectrum was still characteristic of a biphasic system, but this time the phases were both β-gallia phases, the first one with $x \approx 0$ and the other one with $x = 0.15$ (Fig. 6b). The spectra recorded inside the irradiated hole were characteristic of a β-gallia phase with 12% Indium (Figs. 6c to 6e). This proves again a great loss of indium during the laser heating, since the composition is lower than the initial composition (20%).

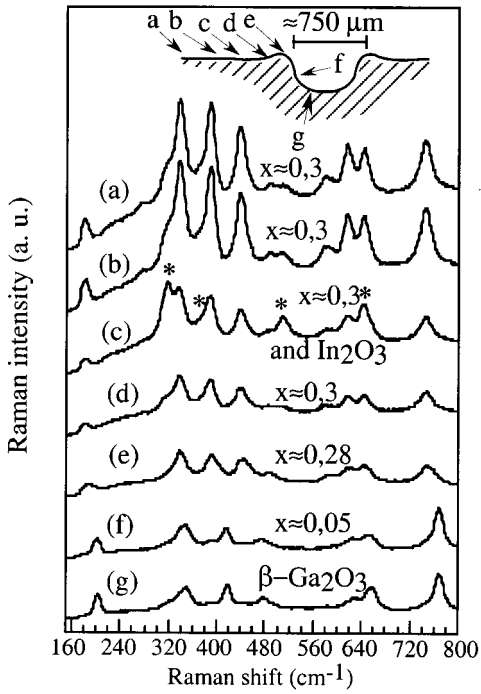

FIG. 7. Study of the melted hole created by laser irradiation of a coprecipitated solid solution of β-$Ga_{2-2x}In_{2x}O_3$ with initial composition $x = 0.35$ heated 2 h at 1200°C. The profile of the hole (approximate diameter, 750 µm) is presented at the top of the figure and the letters a to g indicate the areas where the Raman spectra (a) to (g) were respectively recorded. The stars on spectrum (c) correspond to a cubic phase of In_2O_3.

RECRYSTALLIZATION OF β-$Ga_{2-2x}In_{2x}O_3$ UNDER LASER IRRADIATION

Pellets of β-$Ga_{2-2x}In_{2x}O_3$ solid solutions elaborated by coprecipitation or solid state reaction and heated 2 h at 1200°C were irradiated with a focused ($f = 15$ cm) 6-W multiline argon ion laser emission. Then, the melted holes created under irradiation were studied by Raman microspectroscopy. Figure 7 summarizes the results obtained for a coprecipitated sample with $x = 0.35$. Outside the holes, the spectra are characteristic of solid solutions slightly impoverished in indium and reveal an indium loss during the heating treatment of 2 h at 1200°C (Figs. 7a and 7b). Close to the melted holes, the lines characteristic of the solid solutions are still present, but extra lines characteristic of a cubic solid solution of Ga_2O_3 in In_2O_3 are obtained (Fig. 7c). In the bottom of the hole, the lines are shifted further. This shows an important gradient of indium concentration resulting from a nonuniform indium loss and indicating the existence of strong temperature gradients in the hole during heating. The spectra recorded in the bottom of the holes show that the solid solutions are approximately β-Ga_2O_3, without any trace of indium (Fig. 7g). Here a complete volatilization of indium is observed while in the previous experiment only 40% of the initial amount of indium was lost. This may be related to different distances between the laser and the sample and different focusing conditions in the two experiments leading to a much higher local temperature in the present one. The presence of lines characteristic of a cubic solid solution in the Fig. 7c shows that the indium evaporated under irradiation was redeposited at the nearest cold point of the pellet, just outside the hole. However, chemical analysis by scanning electron microscopy also indicates the existence of indium at the bottom of the holes (point labeled g in Fig. 7). This shows that In_2O_3 is deposited at the bottom of the hole but with an amorphous structure undetectable by Raman spectroscopy, while deposited In_2O_3 is crystallized at the borders of the holes (point labeled c in Fig. 7). Exactly the same results were obtained for samples with composition $x = 0.2$.

EPR OF THE IMPACTED AREAS

All the compounds analyzed in this paper were white or yellow (depending on x value) before laser irradiation. But irradiated areas became blue after laser heating. In the case of β-Ga_2O_3, heating at high temperature is known to create

oxygen vacancies (12, 13). These defects act as shallow donors with ionization energy $E_d \approx 0.04$ eV (12) and release free electrons in the conduction band that are responsible for the blue color. These free electrons can be detected by EPR from 4 to 300 K (14). The EPR spectra of the nonirradiated area and of the irradiated spot were separately recorded for samples of either preformed β-$Ga_{2-2x}In_{2x}O_3$ or simple mixture of In_2O_3 and Ga_2O_3. These two kinds of samples exhibit the same type of EPR response. Figure 8a shows the EPR spectra of irradiated and nonirradiated areas on a sample made of a mixture of 80% Ga_2O_3 and 20% In_2O_3 corresponding to the same mixture analyzed by Raman spectroscopy in Fig. 6. Only the irradiated spot exhibits an EPR signal. This signal is fairly narrow with overall peak-to-peak linewidth of about 1.4 mT and the average g factor is $g_{av} = 1.948$. Actually, the simulation of this signal (Fig. 8a) shows that a slight anisotropy of the g-factor must be considered, with $g_x = 1.952$, $g_y = 1.948$ and $g_z = 1.946$. The intrinsic linewidth of the individual components is about 0.9 mT. The small width of the signal and the g values are consistent with those of free electrons in the conduction band released by oxygen vacancies (5), thus proving the nonstoichiometry and the n-type conducting character of the irradiated spot. A previous investigation of the EPR in β-$Ga_{2-2x}In_{2x}O_3$ solid solutions gave the following linear relation between the average g factor and the composition x (5):

$$g_{av} = 1.9631 - 0.077x. \qquad [2]$$

With the value $g_{av} = 1.948$, Eq. [2] gives the indium content $x \approx 0.2$ in the laser-induced conducting spot. This value is consistent with the initial composition of the mixture but slightly larger than the composition $x \approx 0.12$–0.15 deduced from Raman spectroscopy (Fig. 6). This suggests that different parts of the irradiated spot are probed by EPR and Raman spectroscopy. The weaker loss of indium in the paramagnetic region indicates that the latter was submitted to a lower temperature and thus to a weaker laser intensity. Therefore this region might lie below the one probed by Raman spectroscopy. Another evidence of the delocalized character of the electron spins detected by EPR is the Overhauser shift to low fields exhibited by the EPR signal when the microwave power is increased (Fig. 8b). This shift is characteristic of a dynamic polarization of the nuclear spins (here those of ^{69}Ga, ^{71}Ga, and ^{115}In) interacting with delocalized electron spins upon saturation of the EPR transition of the latter (15). The Overhauser shift ΔB_{ov} as a function of the incident microwave power P follows the relation (16)

$$\Delta B_{ov} = (\Delta B_{ov})_{max} \frac{P}{a + P}, \qquad [3]$$

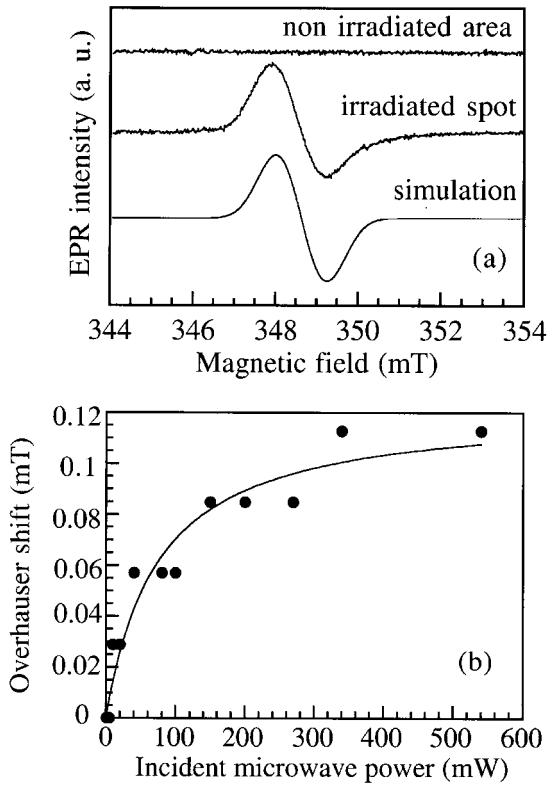

FIG. 8. (a) Room temperature EPR spectra of the sample of Fig. 6 at microwave power $P = 2$ mW. (b) Shift to low fields of the EPR signal in the irradiated spot at $T = 150$ K versus the incident microwave power.

with the maximum Overhauser shift in our case $(\Delta B_{ov})_{max} = 0.12$ mT at $T = 150$ K. The value of $(\Delta B_{ov})_{max}$ primarily depends on the crystallographic and electronic structures of the material, but for a given structure it is driven by disorder (17). The latter enhances nuclear relaxation mechanisms competing with the electron–nucleus cross-relaxation reponsible for the Overhauser shift, so that the higher the disorder, the lower $(\Delta B_{ov})_{max}$. The value $(\Delta B_{ov})_{max} = 0.12$ mT is significantly lower than values $(\Delta B_{ov})_{max} \geq 0.4$ mT obtained for long time annealed β-$Ga_{2-2x}In_{2x}O_3$ compounds (5). Besides, the linewidth $\Delta B_{pp} = 0.9$ mT of the spin packets is significantly larger than the linewidth $\Delta B_{pp} = 0.04$ mT of highly ordered β-Ga_2O_3 single crystals (14). These observations indicate that the irradiated spots suffer from an important disorder presumably related to a heterogeneous composition in indium.

CONCLUSION

A continuous evolution of the Raman spectra was observed in the existence range of the solid solution with β-gallia structure ($x \leq 0.4$), while extra lines characteristic of In_2O_3 appear for $x > 0.4$, consistent with the phase diagram

of the binary system Ga_2O_3–In_2O_3 (3). In addition, the Raman spectrum of the κ-alumina-type phase appearing at high temperature ($T = 1550°C$ in our case) and high indium concentrations ($x > 0.4$) (8, 9) could be detected. In the β-$Ga_{2-2x}In_{2x}O_3$ compounds, the line positions were very sensitive to the indium concentration, thereby allowing the composition of the sample to be determined from the Raman spectra.

It was shown that a laser heating could induce the solid solution formation but with strong local variations of both the oxygen and cationic compositions. The most interesting feature is the important loss of indium upon heating. It is actually known that Ga_2O_3 and In_2O_3 decompose into Ga_2O and In_2O, respectively, at high temperature (18, 19). Since the volatility of In_2O is higher than that of Ga_2O (19), the β-$Ga_{2-2x}In_{2x}O_3$ solid solutions are impoverished in indium. This problem may have implications in the elaboration of the β-$Ga_{2-2x}In_{2x}O_3$ compounds since the final composition after heating may differ by several percent from the initial one. Besides, if films are to be elaborated by sputtering or laser ablation techniques, the changes in composition of the target during the process will lead to inhomogeneities and disorder in the deposited films.

However, the possibility of changing the local composition by a laser impact on a preformed homogeneous β-$Ga_{2-2x}In_{2x}O_3$ solid solution may induce interesting physical properties. Figure 9a summarizes the variation in composition and the different phases around an irradiated zone. As one moves from outside to the center of the irradiated spot, the indium concentration decreases to almost zero but the concentrations of oxygen vacancies and of free electrons increase. The consequences on the local electronic properties are sketched in Fig. 9b. Since the band gap increases when the indium concentration decreases, the system continuously changes from small-gap ($E_g \approx 4.1$ eV for $x = 0.2$ (5)) insulating area outside the irradiated spot to large gap ($E_g \approx 4.7$ eV for $x = 0$ (20)) n-type area inside the spot. Meanwhile, the Fermi level moves from the middle of the gap in the outer area to the bottom of the conduction band in the center of the spot, so that the system is equivalent to an intrinsic/n-type (i–n) junction. Here, we have an example of a local band gap and Fermi level engineering by a continuous change of composition in a single phase. These gradients of composition and of electronic properties actually derive from the temperature gradients generated by a local heating. These gradients are thus controlled by few parameters: the specific heat, the thermal conductivity of the sample, the size and the intensity of the laser beam, and the fraction of light energy converted into heat. For a given material, the first two parameters are fixed so that the i–n junction can be tailored by a proper focusing of the beam and a proper choice of irradiation wavelength.

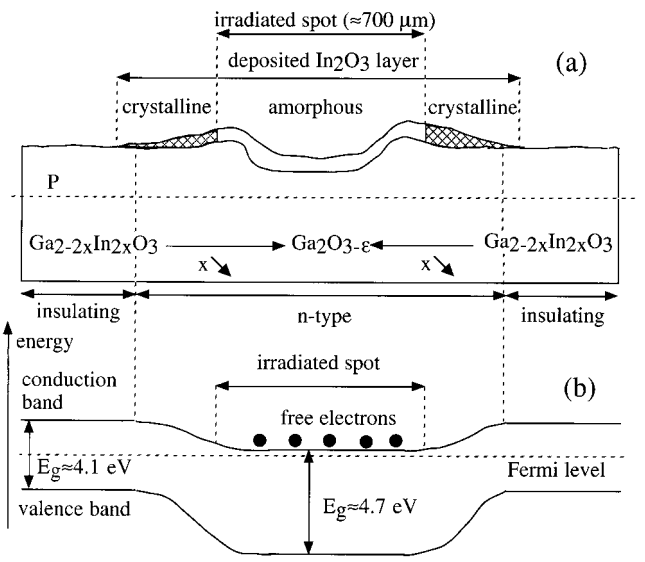

FIG. 9. (a) Schematic picture of a hole created by a laser impact in a pellet of β-$Ga_{2-2x}In_{2x}O_3$ solid solution. (b) Electronic structure in the section plane P.

REFERENCES

1. R. J. Cava, J. M. Phillips, J. Kwo, G. A. Thomas, R. B. van Dover, S. A. Carter, J. J. Krajewski, W. F. Peck, Jr., J. H. Marshall, and D. H. Rapkine, *Appl. Phys. Lett.* **64,** 2071–2072 (1994); J. M. Phillips, J. Kwo, G. A. Thomas, S. A. Carter, R. J. Cava, S. Y. Hou, J. J. Krajewski, J. H. Marshall, W. F. Peck, D. H. Rapkine, and R. B. van Dover, *Appl. Phys. Lett.* **65,** 115–117 (1994); D. D. Edwards, T. O. Mason, F. Goutenoire, and K. R. Poeppelmeier, *Appl. Phys. Lett.* **70,** 1706–1708 (1997); T. Minami, Y. Takeda, T. Kakumu, S. Takata, and I. Fukuda, *J. Vac. Sci. Technol. A* **15,** 958–962 (1997); T. Aoki, A. Suzuki, T. Matsushita, H. Kaimi, and M. Okuda, *Jpn. J. Appl. Phys.* **38,** 4802–4803 (1999).
2. V. I. Vasyltsiv, Ya. I. Rym, and Ya. M. Zakharko, *Phys. Status Solidi B* **195,** 653–658 (1996).
3. D. D. Edwards, P. E. Folkins, and T. O. Maso, *J. Am. Ceram. Soc.* **80,** 253–257 (1997).
4. A. F. Pasquevitch, M. Uhrmacher, L. Ziegler, and K. P. Lieb, *Phys. Rev. B* **48,** 10,052–10,062 (1993).
5. L. Binet, G. Gauthier, C. Vigreux, and D. Gourier, *J. Phys. Chem. Solids* **60,** 1755–1762 (1999).
6. R. D. Shanon and C. T. Prewitt, *J. Inorg. Nucl. Chem.* **30,** 1389–1398 (1968).
7. D. Dohy, G. Lucazeau, and A. Revcolevschi, *J. Solid State Chem.* **45,** 180–192 (1982).
8. S. J. Schneider, R. S. Roth, and J. L. Waring, *J. Res. Nat. Bur. Stand. Sect. A* **65,** 345 (1961).
9. J. Macdonald, J. A. Gard, and F. P. Glasser, *J. Inorg. Nucl. Chem.* **29,** 661–671 (1967).
10. B. Piriou and H. Arashi, *Bull. Mineral.* **103,** 363–366 (1980).
11. J. M. Malézieux and B. Piriou, *Bull. Mineral.* **111,** 649–669 (1988).
12. M. R. Lorentz, J. F. Woods, and R. J. Gambino, *J. Phys. Chem. Solids* **28,** 403–404 (1967).
13. T. Harwig and J. Schoonman, *J. Solid State Chem.* **23,** 205–211 (1978).

14. E. Aubay and D. Gourier, *Phys. Rev. B* **47,** 15,023–15,036 (1993).
15. A. Abragam, *in* "Principles of Nuclear Magnetism," Chap. 9, p. 354. Clarendon Press, Oxford, UK, 1961.
16. C. Ryter, *Phys. Rev. Lett.* **5,** 10–11 (1960); W. Stöcklein and G. Denninger, *Mol. Cryst. Liq. Cryst.* **136,** 335–360 (1986).
17. L. Binet and D. Gourier, *J. Phys. Chem.* **100,** 17,630–17,639 (1966).
18. J. H. W. De Wit, *J. Solid State Chem.* **13,** 192–200 (1975).
19. J. Rasneur, F. Eba, P. Lafollet, and J. P. Delinaire, *Rev. Int. Hautes Temp. Refract. Fr.* **27,** 91–100 (1991).
20. H. H. Tippins, *Phys. Rev.* **140,** A316–A319 (1965).